Available online at www.sciencedirect.com
ScienceDirect
Fuel 87 (2008) 1591–1600
FUEL
www.fuelfirst.com

An exploratory study of alkali sulfate aerosol formation during biomass combustion

Lusi Hindiyarti [a], Flemming Frandsen [a], Hans Livbjerg [a], Peter Glarborg [a,*], Paul Marshall [b]

[a] Department of Chemical Engineering, Technical University of Denmark, DK-2800 Lyngby, Denmark
[b] Department of Chemistry and Center for Advanced Scientific Computing and Modeling, University of North Texas, P.O. Box 305070, Denton, TX 76203-5070, United States

Received 3 April 2007; received in revised form 30 August 2007; accepted 4 September 2007
Available online 25 September 2007

Abstract

It is still in discussion to what extent alkali sulfate aerosols in biomass combustion are formed in the gas phase by a homogeneous mechanism or involve heterogeneous or catalyzed reactions. The present study investigates sulfate aerosol formation based on calculations with a detailed gas phase mechanism. The modeling predictions are compared to data from laboratory experiments and entrained flow reactor experiments available in the literature. The analysis support that alkali sulfate aerosols are formed from homogeneous nucleation following a series of steps occurring in the gas phase. The rate-limiting step may be the oxidation of sulfite to sulfate, rather than the oxidation of SO_2 to SO_3 proposed previously. Even though the proposed model is consistent with experimental observations, experiments in a rigorously homogeneous system are called for to test its validity.

Keywords: Sulfate aerosols; Gas phase; Modeling; Sulfur oxide

1. Introduction

In Denmark, there is a significant amount of straw available as byproducts from farming. Previous experience with combustion of some biomass fuels, including straw, has revealed problems with formation of submicron aerosol particles, deposits, corrosion, and emissions. These problems are closely linked to the chemical composition of the biomass. The content of inorganics in annual biomass fuels is about 5–10% of the total mass, and in straw the alkali content, especially potassium, is very high [1].

The formation of aerosols is not favorable for the environment or for human health, since they affect the health of living creatures. The submicron particles are formed by condensation of volatilized material, mainly alkali salts. Their main constituents are the chlorides and sulfates of the alkali metals. Their formation also has negative effects on the boiler operation because they penetrate particle filters more easily than larger combustion particles, and they are usually accompanied by corrosive deposits on boiler surfaces [2].

The characteristics of aerosols formed in the combustion of different biomass fuels have been reported for a wide range of boiler scales from domestic heat producers to large electricity generation plants [3,4]. The relevance of alkali and chlorine for deposit formation and boiler corrosion was pointed out in several studies [5–8]. Alkali metals may combine with alumino-silicates, causing lower melting temperatures of boiler deposits. Without the presence of the alkali, the boiler deposits do not melt at typical biomass combustion temperatures. Therefore, the presence of alkali will increase the fouling tendency in biomass-fired power plants compared to coal-fired boilers [5,6,9].

Alkali sulfates play an important role in the formation of submicron particle formation [2,3,10,11]. Alkali sulfate is normally present in aerosols formed from biomass

* Corresponding author.
E-mail address: pgl@kt.dtu.dk (P. Glarborg).

0016-2361/$ - see front matter © 2007 Elsevier Ltd. All rights reserved.
doi:10.1016/j.fuel.2007.09.001

combustion [2,3,11] and in experiments using a laboratory flow reactor [12,13]. It is still in discussion as to what extent alkali sulfate aerosol formation is initiated in the gas phase by a homogeneous mechanism or involves a heterogeneous mechanism. Only a small fraction of the equilibrium value for gas phase alkali sulfate is expected to form according to early gas phase kinetic considerations [14]. The work by Steinberg and Schofield [14–16] on homogeneous interactions of sodium and sulfur in the burned gas of flames implied that kinetic limitations ruled out homogeneous Na_2SO_4 formation mechanisms under these conditions. Instead, the formation was reported to be a surface phenomenon, involving condensation of alkali chlorides, followed by reaction with gas phase sulfur species to form sulfates in the condensed phase [14]. However, more recent results from Iisa et al. [13] indicate that the sulfation rate in the condensed phase under combustion conditions is too slow to account for the aerosol formation. A number of studies suggest that sulfate aerosols may be formed in the gas phase by recondensation of alkali, volatilized in the combustion zone [2,3,11,13,17]. According to these studies, the particles are formed from alkali sulfate vapors by homogeneous nucleation of salt seeds, which grow by condensation and coagulation. The process is controlled by chemical reactions in the gas between alkali, chlorine, and sulfur species [2,17]. The formation of aerosol particles by homogeneous nucleation from supersaturated vapors is practically immediate, once a certain threshold of supersaturation is exceeded.

A model of particle formation during cooling of a flue gas from the combustion of fuels rich in volatile alkali species was developed by Christensen et al. [2,3,11,18]. According to that model, sulfate seeds are formed by homogeneous nucleation of K_2SO_4 vapors at approximately 1073 K. When the flue gas cools down, KCl condenses on these nuclei. This suggestion has received some experimental support [12,19].

In a recent study, Glarborg and Marshall [17] proposed a detailed mechanism for a gas phase sulfation process. According to this work, the oxidation of SO_2 to SO_3 is the first and presumably rate-limiting step in the gaseous alkali sulfate formation. The subsequent step was proposed to be an association reaction involving KOH or KCl with SO_3:

$$KOH + SO_3(+M) \rightarrow KHSO_4(+M) \quad (R36)$$

$$KCl + SO_3(+M) \rightarrow KSO_3Cl(+M) \quad (R61)$$

Here, the reaction numbers refer to the listing in Table 3. The alkali complexes formed in these reactions may then participate in a series of shuffle reactions leading to alkali sulfate formation, mainly:

$$KSO_3Cl + H_2O \rightarrow KHSO_4 + HCl \quad (R65)$$

$$KHSO_4 + KCl \rightarrow K_2SO_4 + HCl \quad (R60)$$

The proposed mechanism indicates a fast and efficient gas phase sulfation process, with oxidation of SO_2 being the rate-limiting step rather than alkali transformations. The plausibility of the mechanism depends on the thermal stability of the intermediate alkali complexes in the gas phase (KSO_3Cl and $KHSO_4$), as well as the suggestion that these molecule–molecule reactions are fast due to dipole–dipole interactions [17].

The objective of this study is to investigate further the active mechanism in the sulfate aerosol formation in biomass combustion. Recent advances in our understanding of the SO_2 oxidation chemistry [20–22] and K/Cl/S interactions [17,23] are supplemented with an investigation of plausible novel pathways for gas phase K_2SO_4 formation, based on ab initio methods, to yield an updated detailed reaction mechanism for sulfate formation. Modeling predictions are compared to experimental data on aerosol formation from Iisa et al. [13], Jensen et al. [12], and Jimenez and Ballester [19,24]. These data cover a range of experimental techniques, as well as variations in SO_2 and O_2 inlet concentration, residence time, and temperature time history.

2. Detailed chemical kinetic model

The chemical kinetic model for the gas phase interactions between sulfur, chlorine, and potassium earlier proposed by Glarborg and Marshall [17] is used as basis for the current modeling. The reaction mechanism consists of subsets for H_2/O_2, chlorine chemistry, sulfur chemistry, potassium chemistry and the interactions between these subsets. The importance of homogeneous sulfation pathways not involving SO_3 formation is investigated. Specifically, the K/S/O/H subset of Glarborg and Marshall is extended with the alkali species $KHSO_3$ and KSO_4, which have not previously been considered in modeling, as well as a number of additional elementary reactions.

The thermodynamic data used in the present study are taken from previous work [17,21], except for $KHSO_3$ and KSO_4 and their sodium equivalents, and KO. Ab initio studies by Lee et al. [25] reveal a complex electronic structure for KO, with two electronic states very close in energy to the ground state. Based on the parameters provided by Lee et al., we have evaluated partition functions for each state via the rigid-motor harmonic-oscillator approximation, and combined them to derive the thermochemistry shown in Table 2.

The neutral alkali species $KHSO_3$ and KSO_4 (see Fig. 1) are unknown experimentally, so their properties are predicted via ab initio methods. Details of the approach have been given previously [17]. Briefly, the Gaussian-3 methodology [26], as modified for alkali metals [27], was employed to derive the 0 K molecular energies listed in Table 1. Computations were carried out with the Gaussian 03 program suite [28]. These energies were used to compute the 0 K enthalpy changes for the isodesmic processes

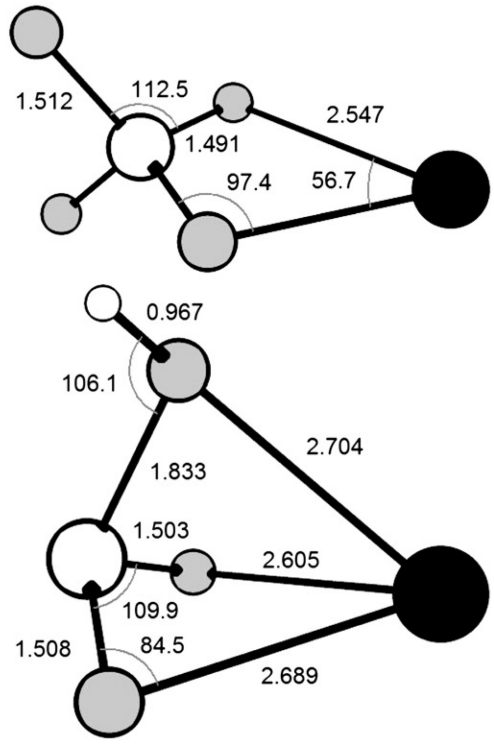

Fig. 1. MB3LYP/6-311G(d,p) geometries computed for KSO_4 and $KHSO_3$. Distances in 10^{-10} m and angles in degrees.

$$OH + AHSO_4 \rightarrow H_2O + ASO_4$$

$$OH + AHSO_3 \rightarrow H_2O + ASO_3$$

The A here represents alkali metal species either as potassium (K) or sodium (Na). Next, moments of inertia and vibrational frequencies scaled by 0.99, computed at the B3LYP/6-311G(d,p) level of theory and given in Table 1, were used to calculate the temperature-dependent heat capacities and other thermodynamic properties (see Table 2), and thus to correct the reaction enthalpies to 298 K. We then used our earlier thermochemistry for $AHSO_4$ and ASO_3 [17], together with values for OH [29] and H_2O [30] to find $\Delta_f H_{298}$ for the unknown species. The C_{2v} structure for ASO_4 shows the binding to a pair of S–O bonds highlighted previously [17] in several other alkali–sulfur species, and is in accord with the calculations of Wang et al. [31]. The $AHSO_3$ molecules exhibit an unusual structure suggestive of binding not only to the two S–O groups but also to the hydroxyl group (see Fig. 1).

The reactions that oxidize SO_2 to SO_3 are of special interest in this study since they have been proposed as possible rate-limiting steps in the K_2SO_4 formation. The sulfur subset was taken from recent work by the authors [20–22] who derived revised rate constants for several reactions important for the SO_2/SO_3 interconversion and validated

Table 1
Ab initio results for alkali metal species

Molecule	*G3* energy (au)[a]	$\Delta H_{f,298}$ (kJ mol^{-1})	Symmetry	Inertia product (GHz^3)	Vibrational frequencies (cm^{-1})[b]
$NaHSO_3$	−786.44191	−668.3	C_1	58.22	129, 166, 306, 322, 417, 454, 498, 579, 990, 1025, 1094, 3750
$NaSO_4$	−860.97449	−655.8	C_{2v} ($^2B_1$)	24.34	84, 219, 282, 327, 384, 427, 515, 580, 765, 915, 1090, 1117
$KHSO_3$	−1224.04538	−690.7	C_1	23.19	117, 149, 235, 304, 396, 427, 494, 572, 990, 1028, 3752
KSO_4	−1298.58048	−698.1	C_{2v} ($^2B_1$)	10.36	58, 173, 215, 333, 370, 430, 513, 564, 762, 918, 1108, 1117

[a] 1 a.u. ≈ 2625.5 kJ mol^{-1}.
[b] B3LYP/6-311G(d,p) result. Frequencies scaled by 0.99.

Table 2
Thermodynamic properties for selected alkali species

Species	$H_{f,298}$	S_{298}	$C_{p,300}$	$C_{p,400}$	$C_{p,500}$	$C_{p,600}$	$C_{p,800}$	$C_{p,1000}$	$C_{p,1500}$	Ref.
K	21.26	34.80	4.97	4.96	4.96	4.97	4.98	4.98	4.98	[17]
KO	13.50	57.45	8.82	8.82	8.82	8.82	8.82	8.82	8.82	[25] (See text)
KO_2	16.00	64.15	11.57	12.13	12.56	12.88	13.27	13.47	13.69	[17]
KOH	−55.41	56.90	11.77	12.21	12.47	12.62	12.83	13.07	13.62	[17]
KCl	−51.27	57.11	8.72	8.85	8.92	8.98	9.04	9.09	9.20	[17]
KSO_2	−95.38	73.46	15.61	16.73	17.55	18.15	18.84	19.16	19.53	[17]
KSO_3	−135.69	78.93	18.54	20.43	21.83	22.83	24.03	24.58	25.23	[17]
KSO_4	−166.84	82.19	22.18	24.86	26.78	28.10	29.56	30.18	31.10	Pw
$KHSO_3$	−165.07	79.63	21.44	23.78	25.46	26.64	27.99	28.66	29.95	Pw
$KHSO_4$	−225.66	83.80	23.73	26.68	28.92	30.57	32.66	33.80	35.42	[17]
K_2SO_4	−261.29	90.14	26.42	29.49	31.63	33.11	34.86	35.81	36.83	[17]
KSO_3Cl	−188.29	86.25	23.33	25.38	26.92	28.06	29.47	30.17	31.01	[17]
$NaSO_4$	−152.47	81.02	21.21	24.10	26.15	27.60	29.25	29.96	30.93	Pw
$NaHSO_3$	−153.27	78.26	20.47	23.04	24.92	26.26	27.83	28.57	29.87	Pw

Units are kcal mol^{-1} ($H_{f,298}$) and cal mol^{-1} K^{-1} (S_{298}, C_p).

Table 3
Rate coefficients for reactions in the potassium subset

No	Reaction	A	n	E	Note
1	$K + O + M \rightleftharpoons KO + M$	1.5E21	−1.50	0	[17] Est
2	$K + OH + M \rightleftharpoons KOH + M$	3.8E19	−0.65	0	[23]
3	$K + HO_2 \rightleftharpoons KOH + O$	1.0E14	0.00	0	[17] Est
4	$K + O_2(+M) \rightleftharpoons KO_2(+M)$	3.6E14	0.00	0	see [17]
	Low pressure limit	5.4E21	−1.32	0	
5	$K + H_2O_2 \rightleftharpoons KOH + OH$	2.5E13	0.00	0	[17] Est[a]
6	$K + H_2O_2 \rightleftharpoons KO + H_2O$	1.6E13	0.00	0	[17] Est[a]
7	$KO + H \rightleftharpoons K + OH$	2.0E14	0.00	0	[17] Est
8	$KO + O \rightleftharpoons K + O_2$	2.2E14	0.00	0	[17] Est[a]
9	$KO + OH \rightleftharpoons KOH + O$	2.0E13	0.00	0	[17] Est
10	$KO + HO_2 \rightleftharpoons KOH + O_2$	5.0E13	0.00	0	[17] Est
11	$KO + H_2 \rightleftharpoons KOH + H$	1.6E13	0.00	0	[17] Est[a]
12	$KO + H_2 \rightleftharpoons K + H_2O$	3.1E12	0.00	0	[17] Est[a]
13	$KO + H_2O \rightleftharpoons KOH + OH$	1.3E14	0.00	0	[17] Est[a]
14	$KO + CO \rightleftharpoons K + CO_2$	1.0E14	0.00	0	[17] Est[a]
15	$KOH + H \rightleftharpoons K + H_2O$	5.0E13	0.00	0	[17] Est
16	$KOH + KOH \rightleftharpoons K_2O_2H_2$	8.0E13	0.00	0	[17] Est
17	$KO_2 + H \rightleftharpoons K + HO_2$	2.0E14	0.00	0	[17] Est
18	$KO_2 + H \rightleftharpoons KO + OH$	5.0E13	0.00	0	[17] Est
19	$KO_2 + H \rightleftharpoons KOH + O$	1.0E14	0.00	0	[17] Est
20	$KO_2 + O \rightleftharpoons KO + O_2$	1.3E13	0.00	0	[17] Est[a]
21	$KO_2 + OH \rightleftharpoons KOH + O_2$	2.0E13	0.00	0	[17] Est
22	$KO_2 + CO \rightleftharpoons KO + CO_2$	1.0E14	0.00	0	[17] Est
23	$K + Cl + M \rightleftharpoons KCl + M$	1.8E20	−1.00	0	see [17]
24	$K + HCl \rightleftharpoons KCl + H$[b]	9.1E12	0.00	1180	see [17]
		1.0E14	0.00	3635	
25	$K + Cl_2 \rightleftharpoons KCl + Cl$	4.4E14	0.00	0	[17] Est[a]
26	$KO + HCl \rightleftharpoons KCl + OH$	1.7E14	0.00	0	[17] Est[a]
27	$KOH + HCl \rightleftharpoons KCl + H_2O$	1.7E14	0.00	0	[17] Est[a]
28	$KO_2 + HCl \rightleftharpoons KCl + HO_2$	1.4E14	0.00	0	[17] Est[a]
29	$KCl + KCl \rightleftharpoons K_2Cl_2$	8.0E13	0.00	0	[17] Est[a]
30	$K + SO_2(+M) \rightleftharpoons KSO_2(+M)$	3.7E14	0.00	0	see [17]
	Low pressure limit	5.2E23	−1.50	0	
31	$K + SO_3(+M) \rightleftharpoons KSO_3(+M)$	3.7E14	0.00	0	[17]
	Low pressure limit	4.7E34	−4.90	0	
32	$KO + SO_2 \rightleftharpoons K + SO_3$	5.0E12	0.00	0	Est
33	$KO + SO_2(+M) \rightleftharpoons KSO_3(+M)$	3.7E14	0.00	0	[17] Est
	Low pressure limit	5.2E23	−1.50	0	
34	$KO + SO_3(+M) \rightleftharpoons KSO_4(+M)$	1.0E14	0.00	0	[17] Est
	Low pressure limit	2.6E42	−7.60	0	
35	$KOH + SO_2(+M) \rightleftharpoons KHSO_3(+M)$	1.0E14	0.00	0	Est as k_{36}
	Low pressure limit	2.6E42	−7.60	0	
36	$KOH + SO_3(+M) \rightleftharpoons KHSO_4(+M)$	1.0E14	0.00	0	[17]
	Low pressure limit	2.6E42	−7.60	0	
37	$KO_2 + SO_2 \rightleftharpoons KO + SO_3$	1.0E14	0.00	0	Est
38	$KO_2 + SO_2(+M) \rightleftharpoons KSO_4(+M)$	1.0E14	0.00	0	Est as k_{36}
	Low pressure limit	2.6E42	−7.60	0	
39	$KSO_2 + O \rightleftharpoons KO + SO_2$	1.3E13	0.00	0	[17] Est
40	$KSO_2 + OH \rightleftharpoons KOH + SO_2$	2.0E13	0.00	0	[17] Est
41	$KSO_2 + OH(+M) \rightleftharpoons KHSO_3(+M)$	2.0E13	0.00	0	Est
	Low pressure limit	1.0E23	−1.50	0	
42	$KSO_2 + O_2(+M) \rightleftharpoons KSO_4(+M)$	1.0E14	0.00	0	Est as k_{36}
	Low pressure limit	2.6E42	−7.60	0	
43	$KSO_2 + KO_2 \rightleftharpoons K_2SO_4$	1.0E14	0.00	0	[17] Est
44	$KSO_3 + O \rightleftharpoons KO + SO_3$	1.3E13	0.00	0	[17] Est
45	$KSO_3 + OH(+M) \rightleftharpoons KHSO_4(+M)$	2.0E13	0.00	0	Est
	Low pressure limit	1.0E23	−1.50	0	
46	$KSO_3 + KO \rightleftharpoons K_2SO_4$	1.0E14	0.00	0	[17] Est
47	$KSO_4 + O \rightleftharpoons KSO_3 + O_2$	1.0E13	0.00	0	Est
48	$KSO_4 + H_2O \rightleftharpoons KHSO_4 + OH$	1.0E14	0.00	0	Est
49	$KSO_4 + KOH \rightleftharpoons K_2SO_4 + OH$	1.0E14	0.00	0	Est
50	$KSO_4 + HCl \rightleftharpoons K_2SO_4 + H$	1.0E14	0.00	0	Est
51	$KSO_4 + KCl \rightleftharpoons K_2SO_4 + Cl$	1.0E14	0.00	0	Est

Table 3 (*continued*)

No	Reaction	*A*	*n*	*E*	Note
52	$KHSO_3 + OH \rightleftharpoons KSO_3 + H_2O$	2.0E13	0.00	0	Est
53	$KHSO_3 + OH \rightleftharpoons KHSO_4 + H$	2.0E13	0.00	0	Est
54	$KHSO_3 + KO \rightleftharpoons KHSO_4 + K$	1.0E14	0.00	0	Est
55	$KHSO_3 + KO_2 \rightleftharpoons KHSO_4 + KO$	1.0E14	0.00	0	Est
56	$KHSO_4 + H \rightleftharpoons KSO_3 + H_2O$	2.0E13	0.00	0	Est
57	$KHSO_4 + O \rightleftharpoons KHSO_3 + O_2$	1.0E13	0.00	0	Est
58	$KHSO_4 + OH \rightleftharpoons KSO_4 + H_2O$	2.0E13	0.00	0	Est
59	$KHSO_4 + KOH \rightleftharpoons K_2SO_4 + H_2O$	1.0E14	0.00	0	[17] Est
60	$KHSO_4 + KCl \rightleftharpoons K_2SO_4 + HCl$	1.0E14	0.00	0	[17] Est
61	$KCl + SO_3(+M) \rightleftharpoons KSO_3Cl(+M)$	1.0E14	0.00	0	[17]
	Low pressure limit	1.9E41	−7.80	0	
62	$KSO_3Cl + H \rightleftharpoons KSO_3 + HCl$	2.0E13	0.00	0	Est
63	$KSO_3Cl + K \rightleftharpoons KSO_3 + KCl$	2.0E13	0.00	0	Est
64	$KSO_3Cl + OH \rightleftharpoons KHSO_4 + Cl$	1.0E14	0.00	0	[17] Est
65	$KSO_3Cl + H_2O \rightleftharpoons KHSO_4 + HCl$	1.0E14	0.00	0	[17] Est
66	$KSO_3Cl + KOH \rightleftharpoons K_2SO_4 + HCl$	1.0E14	0.00	0	[17] Est

Units are cm, mol, s, K.

[a] Estimated to be the same as the measured rate constant for the equivalent sodium reaction.

[b] The resulting rate constant is the sum of the two rate constants.

an updated reaction mechanism against experimental data for SO_2 oxidation over a wide range of conditions. The sulfur subset includes reactions of SO_2 with O, OH, and HO_2 to form SO_3, and reactions involving the $HOSO_2$ intermediate, as well as reactions of SO_3 with the O/H radical pool. All of these reactions may be important for the ratio of SO_2 to SO_3.

The alkali subset of the reaction mechanism is listed in Table 3. Few of the rate constants in this subset have been determined experimentally and estimated values are assigned to most of the reactions [17,23]. Some additional reactions are added to the K/H/S/O subset in the present work. The emphasis has been on reactions of alkali species that either promote oxidation of SO_2 to SO_3 or offer a pathway to potassium sulfate that does not involve SO_3 as intermediate. Formation of SO_3 may be promoted by reactions that replenish the chain carriers in the system. The interaction of alkali species with the O/H radical pool has been investigated in a number of studies [23,32–34]. Under favorable conditions, the alkali metals may participate in the chain-branching sequence

$$KOH(+M) \rightarrow K + OH(+M) \quad (R2b)$$

$$K + H_2O \rightarrow KOH + H \quad (R15b)$$

However, under the conditions of the present study this sequence is not competitive. Alkali species may also promote SO_3 formation by interaction with sulfur oxides. By analogy with reactions of SO_2 with the O/H radical pool, this could occur directly by

$$KO + SO_2 \rightarrow K + SO_3 \quad (R32)$$

$$KO_2 + SO_2 \rightarrow KO + SO_3 \quad (R37)$$

or indirectly through a sequence such as

$$KO + SO_2(+M) \rightarrow KOSO_2(+M)$$

$$KOSO_2 + O_2 \rightarrow KO_2 + SO_3$$

While the direct pathways (R32, R37) are conceivable, the route through $KOSO_2$ is not feasible. $KOSO_2$, with the potassium atom bonded to a single oxygen atom, quickly rearranges to KSO_3 where K is bonded to two O nuclei [17]. The reaction

$$KSO_3 + O_2 \rightarrow SO_3 + KO_2$$

is strongly endothermic and too slow to be of significance. However, KSO_3, formed directly via

$$KO + SO_2(+M) \rightarrow KSO_3(+M) \quad (R33)$$

may promote sulfation through other pathways. Like other alkali molecules KSO_3 has a strong dipole moment and may participate in molecule–molecule reactions, such as

$$KSO_3 + H_2O \rightleftharpoons\rightleftharpoons KHSO_4 + H \quad (R56b)$$

$$KSO_3 + KCl \rightleftharpoons\rightleftharpoons KSO_3Cl + K \quad (R63b)$$

The complexes $KHSO_4$ and KSO_3Cl may then form K_2SO_4 through reactions (R60) and (R65). However, both (R56b) and (R63b) are quite endothermic and slow under the conditions of interest. Another possibility is that KSO_3 form $KHSO_4$ by recombination with hydroxyl radicals,

$$KSO_3 + OH(+M) \rightleftharpoons\rightleftharpoons KHSO_4(+M) \quad (R45)$$

Also KSO_4 may be an intermediate in sulfation pathways that bypasses SO_3, e.g.

$$K + SO_2(+M) \rightarrow KSO_2(+M) \quad (R30)$$

$$KSO_2 + O_2(+M) \rightarrow KSO_4(+M) \quad (R42)$$

$$KSO_4 + KCl \rightarrow K_2SO_4 + Cl \quad (R51)$$

In addition to these reactions, a sequence involving $KHSO_3$ was added to the mechanism

$$KOH + SO_2(+M) \rightarrow KHSO_3(+M) \quad (R35)$$

$$KHSO_3 + O_2 \rightarrow KHSO_4 + O \quad (R57b)$$

followed by conversion of $KHSO_4$ to K_2SO_4 (R60). This sequence is of particular interest, since it only involves reactions between stable species and may constitute a low-temperature pathway to sulfation.

For all added reactions, rate constants were estimated by analogy with other alkali species reactions. The sparse experimental data available, mostly for sodium reactions, indicate that molecule–molecule reactions are generally fast and proceed close to collision frequency, while reactions of alkali species with radicals are somewhat slower [17].

3. Results and discussion

Modeling predictions with the updated detailed gas phase mechanism are compared with experimental data from Iisa et al. [13], Jensen et al. [12] and Jimenez and Ballester [19,24]. The Senkin code [35], which runs in conjunction with Chemkin-II [36], was used in the modeling, assuming plug flow.

The experiments by Iisa et al. [13] were conducted in the temperature range 1173–1373 K in an entrained flow reactor. Solid KCl particles were introduced to the system together with a gaseous mixture of SO_2, O_2, H_2O, and N_2. The residence time of the gases in the reactor was in the range 0.3–1.5 s, after which a quenching system was applied to avoid further reaction. Following Glarborg and Marshall [17], the evaporation of solid potassium chloride was modeled as three-pseudo-first order reactions in series, with rate constants fitted to match the experimental data (Fig. 2).

A comparison between the observed degree of KCl sulfation (symbols) as a function of the residence time at 1173 and 1373 K and modeling predictions (solid lines) is shown in Fig. 3. Considering the uncertainties in both experiments and model, the modeling predictions are in satisfactory agreement with the observed sulfation rate at both temperatures. It is noteworthy that while about 40% of the vaporized KCl forms K_2SO_4 at 1373 K, practically all the KCl vapor is sulfated to K_2SO_4 at 1173 K.

Glarborg and Marshall [17] concluded that the oxidation of SO_2 to SO_3 was the rate-limiting step in the sulfation process. They found their predicted sulfation rate, which was in good agreement with the data of Iisa et al. at 1373 K, to be equal to the SO_3 formation rate. A recent modeling study of sulfation in orujillo (a residue of olive oil production) combustion in an entrained reactor by Jimenez and Ballester [24] supports that the SO_3 formation is rate limiting.

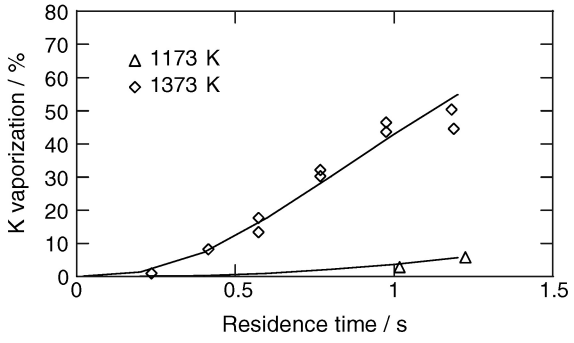

Fig. 2. Vaporization of solid KCl as a function of residence time in an entrained flow reactor at 1173 and 1373 K. Symbols denote experimental results [13], lines denote modeling results. KCl feed rate: 0.24 g/min.

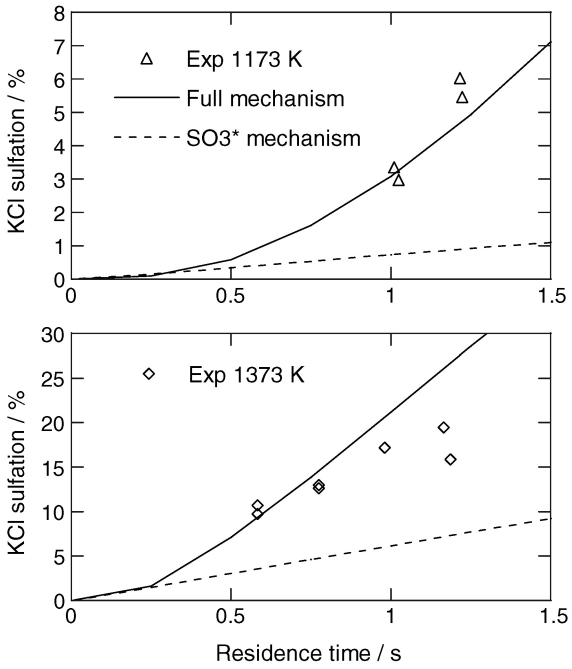

Fig. 3. Conversion of solid KCl to K_2SO_4 as a function of residence time in an entrained flow reactor at 1173 and 1373 K. Symbols denote experimental results [13], while the solid lines denote modeling results with the full mechanism. The dashed lines ("SO_3*") denote predictions where SO_3 formation is assumed rate-limiting, using the updated sulfur chemistry of the present work. Inlet feed contained 2% SO_2, 5% O_2, 10% H_2O, N_2 to balance, and a KCl feed rate of 0.24 g/min.

The dashed lines in Fig. 3 (SO_3*) show modeling predictions assuming that any SO_3 produced in the process instantaneously and irreversibly form potassium sulfate. The simplified mechanism is seen to underpredict the sulfation rate, most pronounced at 1173 K. Both at 1173 and 1373 K, the present sulfur mechanism results in a lower SO_2 oxidation rate and consequently a lower sulfation rate than predicted previously by Glarborg and Marshall [17]. The difference can be attributed to the changes in the sulfur subset implemented in the present work, notably a decrease in $SO_2 + O_2$ reactivity (see below).

The enhanced sulfation rate predicted by the full mechanism compared to SO_3* in Fig. 3 is due to alkali reactions promoting the sulfation rate. In order to identify the key reactions that govern the sulfation rate, a pathway analysis (Fig. 4) and a sensitivity analysis (Fig. 5) for formation of K_2SO_4 were performed for the reaction conditions of Fig. 3 (1373 K), based on computations with the full kinetic model. The main form of gaseous potassium is potassium chloride. In agreement with the previous studies [17,23], some KCl is after vaporization converted to KOH by reaction (Fig. 4)

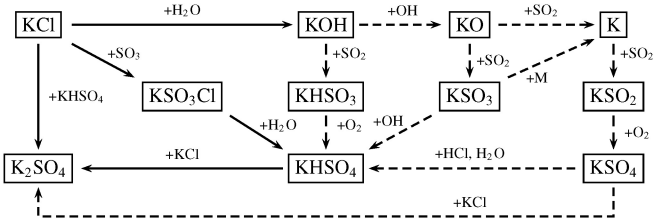

Fig. 4. Pathway diagram for potassium transformations under the conditions of Iisa et al. [13] at 1373 K. The solid lines denote the sulfation mechanism outlined by Glarborg and Marshall [17], while the dashed lines indicate additional pathways proposed in the present work.

$$KCl + H_2O \rightarrow KOH + HCl \quad (R27b)$$

However, KCl remains the dominant gas phase potassium component. Sulfation of KCl is facilitated by SO_3 [17]. The calculations indicate that the reactions involved in the formation of SO_3 are:

$$SO_2 + OH(+M) \rightleftharpoons\rightleftharpoons HOSO_2(+M)$$

$$HOSO_2 + O_2 \rightleftharpoons\rightleftharpoons HO_2 + SO_3$$

$$SO_2 + O(+M) \rightleftharpoons\rightleftharpoons SO_3(+M)$$

$$SO_2 + OH \rightleftharpoons\rightleftharpoons SO_3 + H$$

These reactions all involve radicals and for this reason the oxidation rate for SO_2 is quite sensitive to the generation of chain carriers in the system. At 1173 K, where the O/H radical pool is insignificant, very little SO_3 is formed. The reaction

$$SO_2 + O_2 \rightleftharpoons\rightleftharpoons SO_3 + O$$

proposed earlier [17] to contribute to SO_3 formation, is now known to be too slow to be significant [22]. Once formed, SO_3 promotes sulfation of KCl through the reactions [17]

$$KCl + SO_3(+M) \rightarrow KSO_3Cl(+M) \quad (R61)$$

$$KSO_3Cl + H_2O \rightarrow KHSO_4 + HCl \quad (R65)$$

$$KHSO_4 + KCl \rightarrow K_2SO_4 + HCl \quad (R60)$$

According to the mechanism, reaction (R60) is the main consumption step for $KHSO_4$ and the only reaction of importance that directly produces K_2SO_4. Since these alkali reactions are all fast, none of them shows up in the sensitivity analysis (Fig. 5). Instead, the modeling predictions are sensitive to potassium reactions that either affect chain-branching, promote SO_3 formation, or offer an alternative route to sulfation that bypasses SO_3. The calculations indicate that the presence of potassium may promote SO_3 formation through the sequence

$$KOH + OH \rightarrow KO + H_2O \quad (R13b)$$

$$KO + SO_2 \rightarrow K + SO_3 \quad (R32)$$

The atomic potassium formed in (R32) may further promote sulfation through a sequence involving KSO_2 and KSO_4 as intermediates (Fig. 4):

$$K + SO_2(+M) \rightarrow KSO_2(+M) \quad (R30)$$

$$KSO_2 + O_2(+M) \rightarrow KSO_4(+M) \quad (R42)$$

$$KSO_4 + KCl \rightarrow K_2SO_4 + Cl \quad (R51)$$

$$KSO_4 + H_2O \rightarrow KHSO_4 + OH \quad (R58b)$$

Another sulfation sequence that does not involve SO_3 as an intermediate is

$$KO + SO_2(+M) \rightarrow KSO_3(+M) \quad (R33)$$

$$KSO_3 + OH(+M) \rightarrow KHSO_4(+M) \quad (R45)$$

followed by (R60). These sulfation sequences, with or without SO_3 as an intermediate, all result in the loss of one or two radicals (typically OH) and thus rely on the generation of chain carriers in the system. For this reason they are more active at 1373 K than at 1173 K. However, the 1173 K data of Iisa et al., as well as the data of Jensen et al. [12] discussed below, show that sulfation of KCl readily takes place even at temperatures where formation of radicals in the $SO_2/O_2/H_2O$ system (with or without KCl) is slow or negligible. This imply the existence of a sulfation mechanism that does not require the presence of radicals. Based on the present work, we propose the reaction sequence

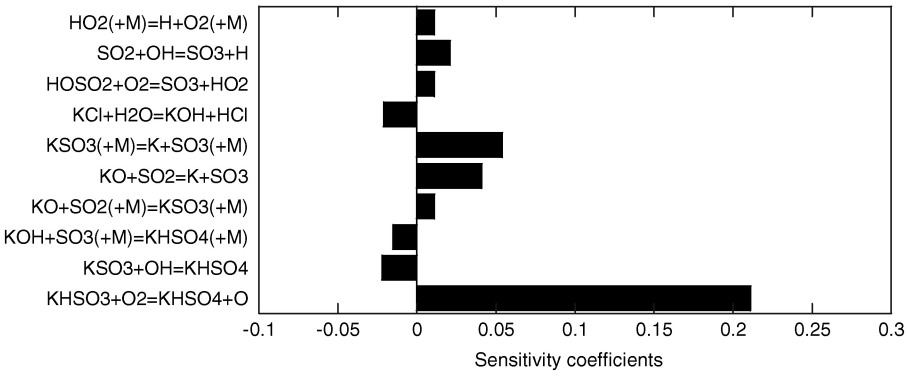

Fig. 5. Sensitivity coefficients for the elementary reactions towards the K_2SO_4 formation for conditions corresponding to Iisa et al. [13] at 1373 K and with a residence time of 1.2 s (Fig. 2).

$$KOH + SO_2(+M) \rightarrow KHSO_3(+M) \quad (R35)$$

$$KHSO_3 + O_2 \rightarrow KHSO_4 + O \quad (R57b)$$

followed by (R60). The reaction (R57) is roughly thermoneutral. This sequence, presently only a hypothesis, is one of several sulfation pathways at 1373 K (Fig. 4), but at 1173 K it is the dominating source of potassium sulfate in the model. Modeling predictions are particularly sensitive to the rate constant for (R57), which is currently only a rough estimate.

The experiments of Iisa et al. were chosen for model evaluation because they were obtained under well-controlled conditions. However, the reaction conditions with high levels of KCl and SO_2 are not representative of practical combustion systems. For this reason, modeling predictions were also compared to the experimental data from Jensen et al. [12] and from Jimenez and Ballester [19]. These studies were conducted under conditions resembling more closely practical combustion systems, with comparatively low concentrations of potassium and sulfur species, as well as a more realistic flue gas cooling rate.

Jensen et al. conducted experiments in a laboratory tubular furnace reactor using a synthetic flue gas containing a mixture of KCl, SO_2, H_2O, O_2, and N_2. The potassium chloride was added to the system by saturating the feed stream or part of it with salt vapors. Downstream of the KCl feeding system (maintained at 1043 K), a peak temperature in the range 1043–1273 K was obtained, followed by cooling of the flue gas at about 300 K/s. Experimental data, presented as the ratio S/(S + Cl) in the collected aerosols downstream, are compared to predicted results in Table 4. The model slightly overpredicts the sulfur content in the aerosols, but the agreement is satisfactory considering the uncertainties. The model correctly predicts that variations in the peak temperature in the range 1043–1273 K have little influence on the sulfation rate. It also captures well the effect of variations in the concentrations of SO_2 and O_2.

According to the calculations, oxidation of SO_2 to SO_3 is negligible under the conditions of Jensen et al. The sulfation occurs almost entirely via the reaction sequence $KCl+H_2O \rightarrow KOH+HCl$ (R27b), $KOH+SO_2(+M) \rightarrow KHSO_3(+M)$ (R35), $KHSO_3+O_2 \rightarrow KHSO_4+O$, (R57b), $KHSO_4+KCl \rightarrow K_2SO_4+HCl$ (R60). The rate-limiting step in this sequence is reaction (R57). If this step is omitted from the mechanism, the predicted sulfation rate is lowered more than an order of magnitude.

Finally, the model is evaluated against experimental data of Jimenez and Ballester [19,24] for combustion of orujillo in an entrained flow reactor. The reactor, maintained at a temperature of 1573 K, was followed by a cooling section with a temperature gradient of ~600 K/s. A comparison between modeling predictions and the observed Cl/S ratio in the aerosols is presented in Fig. 6. The model underpredicts the sulfate formation at very low SO_2 levels, resulting in higher Cl/S values compared to the experimental data. Even though the reactions between SO_2/SO_3 and KOH/KCl occur almost at collision frequency, the sulfation rate is limited due to the very low concentration of reactants (13 ppm KOH, 10–25 ppm SO_2 in the inlet). For this reason, even the SO_3 formed is only partly converted to K_2SO_4 and the model predicts a comparatively low degree of sulfation. However, at higher sulfur concentrations the agreement between modeling predictions and experimental data is satisfactory (see Fig. 6).

In a number of studies on formation of sulfate aerosols [2,3,11–13,17,24,37] it was concluded that SO_3 formation in the gas phase is the rate-limiting step and that immediately after its formation, the SO_3 is consumed to form K_2SO_4. As shown above, a modeling approach based on this assumption underpredicts the formation of sulfate aerosols, in particular at lower temperatures. This discrepancy is not a result of deficiencies in the H/S/O subset of the reaction mechanism. In Fig. 7, modeling predictions are compared to experimental data [38–40] obtained in atmospheric pressure flow reactors with of the order of 1000 ppm SO_2, 4–60% O_2, 0–9% H_2O; with and without presence of combustibles (450 ppm CO). Temperatures were in the range 973–1325 K, with 0.2–10 s residence time. With a

Table 4
Comparison between experimental results from Jensen et al. [12] and modeling predictions for the sulfation of KCl, presented as the ratio S/(S + Cl) in the captured aerosols

Conditions	Sulfur content (exp)	Sulfur content (pred)
	S/(S + Cl)	S/(S + Cl)
	(mol/mol%)	(mol/mol%)
T_{peak} = 1043 K	7.1	10.2
T_{peak} = 1073 K	5.9	10.2
T_{peak} = 1223 K	6.8	10.2
T_{peak} = 1273 K	7.9	10.2
100 ppm SO_2	5.0	6.7
19% O_2	15.9	20.0

The experimental conditions are held constant except for the variation noted in the first column: Peak temperature 1223 K, feed composition: 200 ppm KCl, 200 ppm SO_2, 4% O_2, 4% H_2O, N_2 to balance.

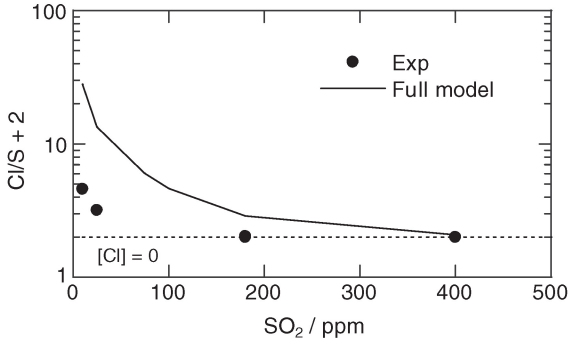

Fig. 6. Comparison of model predictions (solid lines) with the experimental data for the Cl/S ratio in combustion of orujillo in the captured aerosols from Jimenez and Ballester [19] (symbols). Inlet composition: 13 ppm KOH, 34 ppm HCl, 10/ 25/180 ppm SO_2, 5% O_2, 20% H_2O, 8% CO_2 and N_2 to balance.

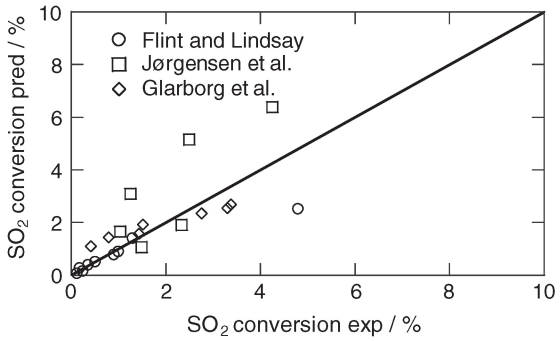

Fig. 7. Correlation between experimental data for the oxidation of SO_2 and modeling predictions with the sulfur subset of the present model. The experimental data were obtained in atmospheric pressure laboratory flow reactors under the following conditions: Flint and Lindsay [38] 1400 ppm SO_2, 8% H_2O, and air to balance at 973–1173 K and 1–10 s residence time; Jørgensen et al. [40] 480 ppm SO_2, 60% O_2, 0–1% H_2O, and N_2 to balance at 1200–1325 K and 4 s residence time; Glarborg et al. [39] 450 ppm CO, 1400 ppm SO_2, 4% O_2, and 1% or 9% H_2O at 1000–1200 K and 0.2 s residence time.

few exceptions the observed conversion of SO_2 is in the range 0–4%. In general, the sulfur subset [22] predicts well the homogeneous SO_2 oxidation over this range of conditions. There are no indications that the model underpredicts oxidation of SO_2; in fact, the most important discrepancy is an overprediction of the oxidation rate for the conditions of Jørgensen et al. [40].

The data of Fig. 7, as well as other literature results [38,41,42], show that the homogeneous oxidation of SO_2 by oxygen molecules at temperatures below 1173 K is very slow. During moist CO oxidation [39] the oxidation rate of SO_2 is enhanced due to the generation of radicals. However, even in the absence of combustibles, an even higher SO_2 consumption is found in SO_2/O_2/alkali metal systems [12,13]. This suggests that the presence of alkali metals may promote oxidation of SO_2. In particular the experimental data of Jensen et al. [12] show high conversion rates for SO_2, in the range 5–16% at temperatures as low as 1043 K. Similar levels of sulfation have been reported from field measurements of straw and other alkali containing biomass fuels [11]. Since homogeneous oxidation of SO_2 to SO_3 cannot account for the observed sulfation of KCl at lower temperatures, the sulfation rate must be controlled either by chemistry involving (stable) K-containing species, as outlined above, or surface reactions.

Several studies have been reported for heterogeneously catalyzed SO_3 formation [37,40,42,43]. Among materials often used in laboratory studies, steel and to a lesser extent alumina have been shown to catalyze oxidation of SO_2, while quartz can be considered inert [40]. In practical combustion systems fly ash is likely to be the most efficient catalyst. It has been observed that submicron-ash may catalyze the SO_2 oxidation to SO_3 in the convective passes of a coal-fired utility boiler, depending on the fuel, combustion conditions, and temperature profile in the convective section [43]. Both the iron oxide content [37,43] and the calcium content [43] of the fly ash are important for the catalytic activity. A laboratory study by Marier and Dibbs [37] showed that the degree of oxidation of SO_2 in the presence of fly ash was 10–30%, increasing linearly with the iron oxide content of the ash, compared to a conversion below 1% in the absence of fly ash. Graham and Sarofim [43] used submicrometer CaO to study the inorganic aerosols and their role in catalyzing sulfuric acid production in furnaces. The sulfation reaction of submicrometer CaO was reported to be fast. Iron oxides on boiler walls and tube furnaces may also be active as catalysts. A study on emissions of sulfur trioxide from coal-fired power plants [44] indicates that formation of SO_3 may be catalyzed by iron oxides at lower temperatures (700–870 K) in the economizer region of the boiler. This formation depends on site-specific factors such as cleanliness of the tube surfaces.

Under the experimental conditions of Jensen et al. [12] with the high reported sulfation levels, there is no indication that catalytic oxidation of SO_2 to SO_3 contributes significantly to the K_2SO_4-formation. The available surfaces include the alumina reactor wall, which is to some extent covered by alkali deposits. However, alumina is not a very active catalyst for SO_2 oxidation [40], and there are no indications of a fast reaction between molten/solid KCl and SO_2 (see [17] and references therein). It has been suggested [45] that presence of K_2SO_4 nuclei may promote additional K_2SO_4 formation in the system, possibly by catalyzing SO_2 oxidation, but to what extent this reaction affects in-flight aerosol formation cannot presently be assessed. For the conditions of Jimenez and Ballester [19,24] the presence of fly ash may be of importance. However, they report that similar results were obtained in ash-free systems [24].

Sulfation of alkali metals is known to proceed readily (but slow) in condensed phase. However, it is unlikely that sulfates, once formed, are released from a surface to the gas phase as aerosols. We believe that alkali sulfate aerosol seeds are formed from homogeneous nucleation following a series of steps occurring in the gas phase. The seeds subsequently act as condensation nuclei for further condensation of alkali sulfate vapors and other supersaturated vapors, e.g., alkali chlorides, as the flue gas cools down. The rate-limiting step is the oxidation of SO_2 S^{IV} to a higher oxidation state. The present work indicate that it may be involve oxidation of sulfite to sulfate, rather than oxidation of SO_2 to SO_3, as proposed previously. Such a mechanism is consistent with experimental observations [12,13,19] as well as with ab initio calculations on the thermal stability of the proposed complex intermediates (present work, [17]) and the observation that molecule–molecule reactions involving alkali species are very fast, proceeding close to collision frequency [17]. The proposed mechanism currently cannot be proven, since reported experimental results are all obtained in systems where surfaces are present, i.e., reactor walls, deposits, and alkali and/or fly ash particles. There are indications that some or all of these surfaces may catalyze oxidation of SO_2 to SO_3, but their role in alkali sulfate aerosol formation is still in discussion.

Experiments in a rigorously homogeneous system are called for to test the proposed gas phase sulfation mechanism.

4. Conclusions

In this study, sulfate aerosol formation was analyzed based on calculations with a detailed gas phase mechanism. The modeling predictions were compared to data from laboratory experiments and entrained flow reactor experiments available in the literature. The analysis supports the idea that alkali sulfate aerosols are formed from homogeneous nucleation following a series of steps occurring in the gas phase. The rate-limiting step may be the oxidation of sulfite to sulfate, rather than the oxidation of SO_2 to SO_3 proposed previously. Even though the proposed model is consistent with experimental observations, additional experimental work is needed in order to gain more insight into the fundamental mechanisms controlling the sulfate aerosol formation.

Acknowledgements

The authors acknowledge support from the CHEC (Combustion and Harmful Emission Control) Research Program, PSO-Elkraft (Grant FU-2207), the Robert A. Welch Foundation (Grant B-1174), the UNT Faculty Research Fund and the National Science Foundation (Grant CHE-0342824), and the National Center for Supercomputing Applications (Grant CHE000015N). Finally, the Otto Mønsted Fund is acknowledged for financing a guest professorship for P.M. at the Technical University of Denmark.

References

[1] Sander B. Biomass Bioenerg 1997;12:177–83.
[2] Christensen KA, Livbjerg H. Aerosol Sci Technol 2000;33:470–89.
[3] Christensen KA, Livbjerg H. Aerosol Sci Technol 1996;25:185–99.
[4] Johansson LS, Tullin C, Leckner B, Sjovall P. Biomass Bioenerg 2003;25:435–46.
[5] Michelsen HP, Frandsen F, Dam-Johansen K, Larsen OH. Fuel Proc Technol 1998;54:95–108.
[6] Heinzel T, Siegle V, Spliethoff H, Hein KRG. Fuel Proc Technol 1998;54:109–25.
[7] Hansen LA, Nielsen HP, Frandsen FJ, Dam-Johansen K, Hørlyck S, Karlsson A. Fuel Proc Technol 2000;64:189–209.
[8] Nielsen HP, Frandsen FJ, Dam-Johansen K, Baxter LL. Prog Energ Combust Sci 2000;26:283–98.
[9] Boow J. Fuel 1972;51:170–3.
[10] Latva-Somppi J, Moisio M, Kauppinen EL, Valmari T, Ahonen P, Keskinen J. J Aerosol Sci 1998;29:461–80.
[11] Christensen KA, Stenholm M, Livbjerg H. J Aerosol Sci 1998;29(4):421–44.
[12] Jensen JR, Nielsen LB, Schultz-Møller C, Wedel S, Livbjerg H. Aerosol Sci Technol 2000;33:490–509.
[13] Iisa K, Lu Y, Salmenoja K. Energ Fuel 1999;13:1184–90.
[14] Steinberg M, Schofield K. Prog Energ Combust Sci 1990;16:311–7.
[15] Schofield K, Steinberg M. J Phys Chem 1992;96:715–26.
[16] Steinberg M, Schofield K. Combust Flame 2002;129:453–70.
[17] Glarborg P, Marshall P. Combust Flame 2005;141:22–39.
[18] Christensen KA. PhD thesis. Technical University of Denmark, ISBN 87-90142-04-7; 1995.
[19] Jimenez S, Ballester J. Combust Flame 2005;140:346–58.
[20] Yilmaz A, Hindiyarti L, Jensen A, Glarborg P, Marshall P. J Phys Chem A 2006;110:6654–9.
[21] Rasmussen CL, Glarborg P, Marshall P. Proc Combust Inst 2007;31:339–47.
[22] Hindiyarti L, Glarborg P, Marshall P. J Phys Chem A 2007;111:3984–91.
[23] Hindiyarti L, Frandsen F, Livbjerg H, Glarborg P. Fuel 2006;85:978–88.
[24] Jimenez S, Ballester J. Fuel 2007;86:486–93.
[25] Lee EPF, Soldan P, Wright TG. J Chem Phys 2002;117:8241.
[26] Curtiss LA, Raghavachari K, Redfern PC, Rassolov V, Pople JA. J Phys Chem 1998;109:7764.
[27] Curtiss LA, Redfern PC, Rassolov V, Kedziora G, Pople JA. J Chem Phys 2001;114:9287.
[28] Frisch MJ, Trucks GW, Schlegel HB, Scuseria GE, Robb MA, Cheeseman JR, et al. Gaussian 03, revision D. 02. Wallingford, CT: Gaussian, Inc.; 2004.
[29] Ruscic B, Wagner AF, Lawrence LB, Harding LB, Asher LR, Feller D, et al. J Phys Chem A 2002;106:2727.
[30] Gurvich LV, Bergman GA, Gorokhov LN, Iorish VS, Leonidov VYa, Yungman VS. J Phys Chem Ref Data 1997;26:1031–110.
[31] Wang X-B, Ding C-F, Nicholas JB, Dixon DA, Wang L-S. J Phys Chem A 1999;103:3423.
[32] Perry RA, Miller JA. Int J Chem Kinet 1996;28:217–34.
[33] Zamansky VM, Lissianski VV, Maly PM, Ho L, Rusli D, Gardiner Jr WC. Combust Flame 1999;117:821–31.
[34] Glarborg P. Proc Combust Inst 2007;31:77–98.
[35] Lutz AE, Kee RJ, Miller JA. A Fortran program for predicting homogeneous gas phase chemical kinetics with sensitivity analysis. Sandia National Laboratories, Report SAND87-8248; 1987.
[36] Kee RJ, Rupley F, Miller JA. Chemkin ii – a Fortran chemical kinetics package for the analysis of gas phase chemical kinetics. Sandia National Laboratories, Report SAND89-8009; 1989.
[37] Marier P, Dibbs HP. Thermochim Acta 1974;8:155–65.
[38] Flint D, Lindsay AW. Fuel 1952;30:288.
[39] Glarborg P, Kubel D, Dam Johansen K, Chiang HM, Bozzeli JW. Int J Chem Kinet 1996;28:773–90.
[40] Jørgensen TL, Livbjerg H, Glarborg P. Chem Eng Sci 2007;62:4496–9.
[41] Cullis CF, Mulcahy MFR. Combust Flame 1972;18:225–92.
[42] Dennis JS, Hayhurst AN. Combust Flame 1988;72:241–58.
[43] Graham KA, Sarofim AF. J Air Waste Manage Assoc 1998;48:106–12.
[44] Srivastava RK, Miller CA, Erickson C, Jambhekar R. J Air Waste Manage Assoc 2004;54(6):750–62.
[45] Zeuthen J. PhD thesis. Technical University of Denmark; 2007.